Int. J. Heat Mass Transfer. Vol. 36, No. 14, pp. 3449–3458, 1993
Printed in Great Britain

0017–9310/93 $6.00 + 0.00

Nonequilibrium evaporation of molten-metal drops in an alternating magnetic field

YILDIZ BAYAZITOGLU and ROBERT CERNY
Department of Mechanical Engineering and Materials Science, Rice University, Houston, TX 77251-1892, U.S.A.

(*Received* 17 *July* 1992 *and in final form* 10 *February* 1993)

Abstract—A lumped analysis of molten-metal droplets moving in an inhomogeneous magnetic field and evaporating in inert-gas surroundings by using three nonequilibrium evaporation models is performed. Results show marked differences (up to 1000 K) in drop temperatures for the diffusion and vacuum-like, high-velocity models but relatively low differences (less than 8%) in the final size of the drop radius. A quasi-steady diffusion–convection model accounting for finite relative velocity of droplets with respect to the ambient gas is considered as an intermediate case between these two limits. Ambient gas flowing opposite to the direction of droplet motion can improve the efficiency of the evaporation process.

1. INTRODUCTION

EVAPORATION of liquid drops in gaseous surroundings has been an object of extensive study for years. First studies in this area appeared in the second half of the last century and in the beginning of this century in an effort to explain natural phenomena such as the cycle of water in Nature. Some of the researchers during this period were Maxwell, Stefan, Langmuir and others. Early work on this problem was reviewed by Fuchs [1].

In the course of the 20th century, the technical applications of the evaporation process began to increase. Vaporization of fuel droplets, cooling of hot gases by a spray of water, drying of viscous solutions by atomization, to name a few, became important in engineering research. A representative review of the combustion of single fuel droplets in an oxidizing atmosphere prior to 1973 has been made by Williams [2]. The problem of single-droplet quasi-steady diffusion-controlled vaporization has been extensively studied by Kent [3] for water and hydrocarbon liquids. Other reviews in the combustion area have outlined extensive research work done after 1973, e.g. Faeth [4], Law [5], Sirignano [6]. Different vaporization models in the combustion area were analyzed, e.g. by Prakash and Sirignano [7], Aggarwal *et al.* [8], Abramzon and Sirignano [9] and others.

Among the most recent publications, Aggarwal *et al.* [10] have studied multicomponent vaporization of fuel droplets, Berlemont *et al.* [11] have solved the influence of fluid turbulence on droplet evaporation. In the area of non-combustion evaporation Tang and Munkelwitz [12] investigated evaporation of glycerol and oleic acid, Zhang and Gogos [13] studied film evaporation of water and *n*-heptane in air.

In general, most of the work in both theoretical and experimental investigations of the evaporation process was done with water and organic droplets. Evaporation of metals has not been studied as frequently. In the modeling of welding processes, for example Block-Bolten and Eagar [14] investigated pool evaporation of aluminum alloys and stainless steel by arc welding. More recently DebRoy *et al.* [15] modeled vaporization of liquid metal pools induced by industrial welding lasers.

The use of electromagnetic vaporization for size reduction of metal droplets was studied by Bayazitoglu and Cerny [16] as a prospective method in powder metallurgy. In refs. [16, 17], the electromagnetic vaporization process was solved in the heat-conduction and infinite-conductivity limits for a solitary static metal droplet and stagnant ambient gas. Later, an infinite-conductivity model for metal droplets moving in an inhomogeneous magnetic field was formulated in refs. [18, 19]. Both these models assumed equilibrium vaporization and brought to light different features from the classical hot-air vaporization models used in combustion problems, for instance, limitations on the final droplet size and infinite droplet lifetime.

In this paper, we deal with nonequilibrium vaporization of molten-metal drops assuming moving droplets with infinite thermal conductivity. We formulate two limiting cases in the determination of evaporation rate. The fastest vacuum-like evaporation model assumes a high velocity of ambient gas, while the slowest diffusion model considers no motion of the ambient gas relative to the droplet. We also analyze the influence of ambient-gas velocity between these two limits using a quasi-steady approximation to the evaporation rate and compare our results with those obtained by the equilibrium model from ref. [19].

2. MODEL OF EVAPORATING DROPLETS

We consider the characteristic volume V_c of the vaporization chamber that contains a single liquid metal droplet. Assuming homogeneous distribution of droplets of the same size in the chamber we can

NOMENCLATURE

a acceleration [m s^{-2}]
amu atomic mass unit [kg]
B magnetic induction [T]
c specific heat [J kg^{-1} K^{-1}]
C concentration
d molecule diameter [m]
D diffusion coefficient [m^2 s^{-1}]
F force [N]
g gravity acceleration [m s^{-2}]
G gravity force [N]
h heat transfer coefficient [W m^{-2} K^{-1}]
I amplitude of electric current [A]
j mass flux [kg m^{-2} s^{-1}]
k thermal conductivity [W m^{-1} K^{-1}]
k_B Boltzmann constant [J K^{-1}]
l length [m]
L latent heat [J kg^{-1}]
m mass [kg]
$m_{1,2}$ mass of molecules 1,2 [kg]
M molar mass [kg mol^{-1}]
n number of turns per unit length [m^{-1}]
N number of molecules per unit volume [m^{-3}]
p pressure [Pa]
P power [W]
$\mathbf{r}$ position vector [m]
R radius of the drop [m]
R_g molar gas constant [J mol^{-1} K^{-1}]
R_S radius of the solenoid [m]
Re Reynolds number
dR/dt interface velocity [m s^{-1}]
s shape factor [m]
S surface [m^2]
Sc Schmidt number
Sh Sherwood number
t time [s]
t temperature [K]
v velocity [m s^{-1}]
V volume [m^3].

Greek symbols
β empirical coefficient
β_c volume thermal expansion coefficient [K^{-1}]
δ skin depth [m]
ε emissivity
μ permeability [H m^{-1}]
ν kinematic viscosity [m^2 s^{-1}]
ρ density [kg m^{-3}]
σ electrical conductivity [Ω^{-1} m^{-1}]
σ_{SB} Stefan–Boltzmann constant [W m^{-2} K^{-4}]
ω radian frequency [s^{-1}].

Subscripts
b boiling
B buoyancy
c characteristic volume
d drop
e surroundings
em electromagnetic
f final
F frictional
g gas
l limiting value
L liquid
m melting
M metal
max maximum value
o initial value
r relative
s surface
S solenoid
t threshold
v vapor
vap vaporization.

write

$$V_c = \frac{V_d}{C_M}. \tag{1}$$

In the first approximation, we assume $C_M \ll 1$ and a fast removal of both the evaporated metal and heated-up ambient gas from the characteristic volume, e.g. by flowing ambient gas. The mixture of ambient gas and metal vapor inside V_c can be then considered to have the same composition and properties in time and

$$T_c(\mathbf{r}, t) = T_\infty = \text{const.} \tag{2}$$

$$\rho_v(\mathbf{r}, t) = \rho_\infty = \text{const.} \tag{3}$$

2.1. *Motion of the droplets*

Under the above assumptions, we can only deal with one characteristic droplet moving through the vaporization chamber. The initial conditions are: the position and velocity vectors of the drop are $\mathbf{r}(0) = \mathbf{r}_0$, and $\mathbf{v}(0) = \mathbf{v}_0$, respectively, the drop radius is $R(0) = R_0$, the drop temperature is $T(\mathbf{r}, 0) = T_0$, where $T_m < T_0 < T_b$. The alternating magnetic field inside the vaporization chamber has the form

$$\mathbf{B}(\mathbf{r}) = \mathbf{B}_0(\mathbf{r}) \cdot e^{j\omega t}. \tag{4}$$

The amplitude $\mathbf{B}_0(\mathbf{r})$ and the radian frequency ω are constant during the vaporization procedure. At the time $t > 0$, there are four main forces acting on the drop: gravitational force $\mathbf{G}$, the buoyancy force $\mathbf{F}_B$, the frictional-resistance $\mathbf{F}_F$ and the electromagnetic force $\mathbf{F}_{em}$. These forces determine the motion of the droplet through the device.

Induced eddy currents heat the drop, and if the

absorbed energy is higher than heat losses due to conduction, convection and radiation, the temperature of the drop will increase. At the same time, if the saturation density of metal vapor corresponding to the drop temperature T is higher than ρ_∞, the drop will evaporate.

The simultaneous heating and evaporation of the droplet will continue until the value of the amplitude of the magnetic induction $\mathbf{B}_0(\mathbf{r})$ at the instantaneous position of the droplet decreases below a certain limit. Then, the temperature of the droplet begins to decrease and evaporation slows down. Finally, the drop leaves the vaporization chamber, the rate of cooling increases rapidly and evaporation becomes negligible.

Assuming the lumped-temperature approximation inside the droplet, we can write the volume heat balance in the form

$$\rho_L L_v \frac{dV_L}{dt} = -P + m_L c_L \frac{dT}{dt} + S_L[h(T-T_\infty)+\varepsilon\sigma_{SB}(T^4-T_\infty^4)]. \quad (5)$$

The equation of motion of the droplet is

$$\frac{d(m_L\mathbf{v})}{dt} = \mathbf{F}_{em}+\mathbf{G}+\mathbf{F}_B+\mathbf{F}_F. \quad (6)$$

The position and velocity of a point mass can be expressed by the kinematic relations

$$\mathbf{r}(t) = \mathbf{r}_0+\mathbf{v}_0 t+\int_0^t\int_0^t \mathbf{a}(t)\,dt^2 \quad (7)$$

$$\mathbf{v}(t) = \mathbf{v}_0+\int_0^t \mathbf{a}(t)\,dt, \quad (8)$$

the radius R and the temperature of the droplet are

$$R(t) = R_0+\int_0^t \frac{dR}{dt}dt \quad (9)$$

$$T(t) = T_0+\int_0^t \frac{dT}{dt}dt. \quad (10)$$

Next, we assume a small drop size and small irregularities in the shape of the drop. This allows us to make the assumption of spherical drops and permits a lumped analysis. Thus assuming spherical drops and substituting for the forces in (6), equations (5) and (6) can be rewritten in a more convenient form with the interface velocity dR/dt and the acceleration of the droplet $\mathbf{a}$ on the left-hand sides,

$$\frac{dR(t)}{dt} = -\frac{3H(x)B_0^2}{4R(t)\rho L_v\sigma\mu^2}+\frac{c_L}{L_v}\frac{R(t)}{3}\frac{dT}{dt} + \frac{1}{\rho_L L_v}[h(T-T_\infty)+\varepsilon\sigma_{SB}(T^4-T_\infty^4)] \quad (11)$$

$$\mathbf{a} = -\frac{3}{2\rho_L\mu}G(x)(\mathbf{B}_0\cdot\nabla)\mathbf{B}_0 + \left(1-\frac{\rho_e}{\rho_L}\right)g-\frac{9}{2}\frac{\rho_e\nu_e}{\rho R(t)^2}\mathbf{v}_r-\frac{3}{R(t)}\mathbf{v}\frac{dR(t)}{dt}, \quad (12)$$

where the values $\mathbf{F}_{em}$ and P were taken from ref. [20] with

$$G(x) = 1-\frac{3}{2x}\frac{\sinh 2x-\sin 2x}{\cosh 2x-\cos 2x}$$

$$H(x) = \frac{x(\sinh 2x+\sin 2x)}{\cosh 2x-\cos 2x}-1$$

$$x = \frac{R}{\delta},\quad \delta = \sqrt{\left(\frac{2}{\omega\mu\sigma}\right)},$$

the relative velocity $\mathbf{v}_r$ of the droplet with respect to the ambient gas is

$$\mathbf{v}_r = \mathbf{v}-\mathbf{v}_g.$$

Now, we have six equations (7)–(12) for the seven variables $\mathbf{r}$, $\mathbf{v}$, $\mathbf{a}$, R, dR/dt, T, dT/dt. The last equation necessary is the relation

$$\frac{dR(t)}{dt} = f(T), \quad (13)$$

that describes the evaporation kinetics on the drop surface.

2.2. *Interfacial kinetics of the vaporization front*

There are several ways to obtain equation (13). As an upper limit to the interface velocity dR/dt, evaporation into vacuum can be considered. This case corresponds with the very high flow rates of the ambient gas when the width of the diffusion boundary layer is less than the mean free path of the molecules of the vapor and practically all the evaporating molecules are carried away by the flowing gas.

According to the kinetic theory of gases [21], the mass flux j_v of the vapor can be expressed

$$j_v = \tfrac{1}{4}\rho_v\bar{v}. \quad (14)$$

The arithmetical average velocity of molecules $\bar{v}$ is given by the relation

$$\bar{v} = \sqrt{\left(\frac{8R_gT}{\pi M}\right)}, \quad (15)$$

where T is the absolute temperature. From the equation of state for an ideal gas the density of vapor is given by ρ_v

$$\rho_v = \frac{p_v M}{R_g T}. \quad (16)$$

Substituting (15) and (16) into (14), we get the mass flux in the form

$$j_v = \sqrt{\left(\frac{M}{2\pi R_g T}\right)}\cdot p_v. \quad (17)$$

The equilibrium vapor pressure of metals p_{eq} for the temperatures between the melting and boiling point can be written [22] as

$$\log p_{eq} = -\frac{A}{T} + B + C \log T, \tag{18}$$

where p_{eq} is measured in mm Hg or

$$p_{eq} = F \cdot T^{C} \cdot 10^{-(A/T)+B}, \tag{19}$$

where p_{eq} is in Pa and the conversion factor $F = 133.32$. Denoting

$$X = F \cdot \sqrt{\left(\frac{M}{2\pi R_g}\right)} \tag{20}$$

and substituting (19) and (20) into (17) we get

$$j_v = X \cdot T^{C-0.5} \cdot 10^{-(A/T)+B}. \tag{21}$$

The mass flux due to evaporation from the surface of the drop can be expressed in terms of interface velocity as

$$j_v = -\rho_L \frac{dR(t)}{dt}. \tag{22}$$

Comparing (22) and (21) we finally arrive at the dependence of the interface velocity on the temperature

$$\frac{dR(t)}{dt} = -\frac{X}{\rho_L} \cdot T^{C-0.5} \cdot 10^{-(A/T)+B}. \tag{23}$$

Note that in the nonequilibrium vaporization model, this relation or another relation of the form (13) replace the local thermodynamic equilibrium condition

$$T = T_{vap} = \text{const.}$$

The lower limit to the interface velocity dR/dt is diffusion-driven evaporation. This case is characteristic for very small droplets, where the mass loss consists essentially of diffusion through a film of relatively stationary gas around the droplet. In other words, the concentration gradient of the metal vapor close to the surface is so large that the mass of vapor carried by diffusion is much greater than that carried by convection.

The rate of loss of mass of small droplets can be expressed according to Langmuir [23]

$$-\frac{dm_L}{dt} = s \int_{\rho_\infty}^{\rho_s} D \, d\rho. \tag{24}$$

For a spherical shell the shape factor s is [23]

$$s = \frac{4\pi R R_c}{R_c - R}. \tag{25}$$

For $R \ll R_c$

$$s = 4\pi R. \tag{26}$$

The first approximation to (24) can be written

$$-\frac{dm_L}{dt} = 4\pi R D(\rho_s - \rho_\infty). \tag{27}$$

Substituting for m_L we arrive at

$$\frac{dR}{dt} = -\frac{D}{\rho_L R}(\rho_s - \rho_\infty). \tag{28}$$

If we assume, according to ref. [23] that ρ_s is the volume mass corresponding to the saturation pressure of the metal vapor at the temperature equal to the temperature of the droplet, using (16) and (19) leads to the relation

$$\rho_s = Z \cdot T^{C-1} \cdot 10^{-(A/T)+B}, \tag{29}$$

where

$$Z = F \frac{M}{R_g}.$$

Equation (28) then reads

$$\frac{dR}{dt} = -\frac{D}{\rho_L R}(Z \cdot T^{C-1} \cdot 10^{-(A/T)+B} - \rho_\infty). \tag{30}$$

The solution of intermediate cases falling between these two limits is usually considered in a form analogous to the heat transfer [1, 24, 25]

$$Sh = 2(1 + \beta Re^{1/2} Sc^{1/3}) \tag{31}$$

where $Re = 2Rv/\nu_c$, $Sc = \nu_c/D$. The Sherwood number Sh can be written [1]

$$Sh = -\frac{2R\frac{dm_L}{dt}}{DS(\rho_s - \rho_\infty)}. \tag{32}$$

Substituting for Sh, Re, Sc and m_L in (31) we obtain

$$\frac{dR}{dt} = -\frac{D}{\rho_L R}(\rho_s - \rho_\infty)\left(1 + \beta\sqrt{\left(\frac{2vR}{\nu_c}\right)}\sqrt[3]{\left(\frac{\nu_c}{D}\right)}\right), \tag{33}$$

where β is a constant determined by experiments. Assuming that ρ_s is the volume mass of metal vapor corresponding to the saturation pressure, as before, we finally arrive at

$$\frac{dR}{dt} = -\frac{D}{\rho_L R}\left(1 + \beta\sqrt{\left(\frac{2vR}{\nu_c}\right)}\sqrt[3]{\left(\frac{\nu_c}{D}\right)}\right) \times (Z \cdot T^{C-1} \cdot 10^{-(A/T)+B} - \rho_\infty). \tag{34}$$

Note that equation (34) for diffusion–convection driven evaporation includes the diffusion limit (30) with $v = 0$.

3. MATERIAL PARAMETERS

The vaporization process described in the previous section was simulated for copper drops with argon at atmospheric pressure as the ambient gas. Basic material parameters used in our model are shown in

Table 1. Material parameters

Parameter	Value	Reference
c_L (J kg^{-1} K^{-1})	495	[22]
ρ_L (kg m^{-3})	8000	[22]
$\sigma(T)$ (Ω^{-1} m^{-1})	$(5.0\text{–}3.95)\times10^{6}$ (see Table in Ref.)	[22]
T_m (K)	1356.5	[27]
T_b (K)	2839	[27]
L_v (J kg^{-1})	4.73×10^{6}	[27]
ε	0.12	[28]
ρ_e (kg m^{-3})	1.784	[27]
ν_e (m^2 s^{-1})	1.34×10^{-5}	[27]
k_e (W m^{-1} K^{-1})	1.63×10^{-2}	[27]
β_e (K^{-1})	3.66×10^{-3}	[27]

Table 1. The constants in the equation (23) for copper are [22] $A = 17650$, $B = 13.39$, $C = -1.273$, $X = 4.649$. The diffusion coefficient D of metal vapor in inert gases is not a well measured quantity. Therefore, we used the general relation derived on the basis of the kinetic theory of nonuniform gases [26]. In the first approximation, the diffusion coefficient in a binary mixture considering the model of rigid elastic spheres can be written

$$D = \frac{3}{8(N_1+N_2)d_{12}}\sqrt{\left(\frac{k_B T(m_1+m_2)}{2\pi m_1 m_2}\right)}. \quad (35)$$

For copper and argon we have $m_{Cu} = 63.54$ amu, $m_{Ar} = 39.95$ amu, $d_{Cu} = 2.55\times10^{-10}$ m, $d_{Ar} = 3.82\times10^{-10}$ m. The empirical coefficient β in the relation (34) was chosen according to the recommendations of Soo [25] as $\beta = 0.276$. The heat transfer coefficient h for mixed convection is [29]

$$h = \frac{k_e}{2R}\left\{2+0.493\sqrt{\left(\frac{2v_r R}{\nu_e}\right)} \times\left[1+0.448\left(\frac{2\beta_e g(T-T_\infty)R}{v_r^2}\right)^{0.875}\right]^{1/3.5}\right\}. \quad (36)$$

The values of β_e, k_e, ν_e are shown in Table 1. For the evaluation of frictional drag in equation (12), we used Stokes law as a first approximation. This approximation is valid since in our model the majority of vaporization occurs in the upper portion of the vaporization chamber where droplet velocities are 'small' ($\ll 1.0$ m s^{-1}). When the droplet velocity has become appreciable, the radius of the drop has decreased significantly (from 10^{-4} to 10^{-6} m). Hence, flow remains within the Stokes regime.

4. COMPUTATIONAL RESULTS

In our computer code, the external alternating magnetic field was generated by a helical solenoid. For most of the computations, the length of the solenoid was chosen to be $l_S = 1$ m, the radius $R_S = 0.05$ m and the number of turns per unit length $n_S = 200$ m^{-1}. The drop was initially at rest just above the top of the solenoid, placed on its longitudinal axis, and then it was allowed to fall through the solenoid.

The basic set of computations was performed for the amplitude of alternating current in the solenoid $I_o = 500$ A, the radian frequency $\omega = 2\pi\times10^7$ s^{-1} and drop radius $R_o = 10^{-4}$ m. The temperature of ambient argon was $T_\infty = 300$ K, the volume density of metal vapor in argon $\rho_\infty = 0$, the velocity of ambient $v_p = 0$.

First, we analyzed the influence of the three different models of the interfacial kinetics—the vacuum-like high-velocity model (HVM), represented by equation (23), the diffusion model (DM), equation (30), and diffusion–convection model (DCM), equation (34)—on the principal parameters of the vaporization process, i.e. the functions $R(t)$, dR/dt, and $T(t)$ for the same external conditions. We investigated the process at temperatures higher than the melting point because for most metals, evaporation from the solid phase is negligible in our time scale. Thus, we started our computations at $T = T_m$ and finished them when $T = T_m$ was reached again after the drop fell through the solenoid.

Figure 1(a) shows that the temperature histories of the drop have similar qualitative character for all three models. In the first phase of heating, most of the absorbed heat is spent to raise the temperature of the drop. The net evaporation rate is relatively low at lower temperatures and the only way to increase it is by increasing the drop temperature. Therefore, the initial phases of the vaporization process are in fact very similar in all the models. After a certain amount of time, the maximum value of the drop temperature is reached and the vaporization almost reaches equilibrium. In a relatively long time interval (60–70% of the vaporization time in our case), the temperature decreases very slowly creating a near-plateau on the $T(t)$ curves. This is a consequence of the fact that inside a solenoid with a high ratio l_S/R_S as in our configuration, the magnetic field along the z-axis changes relatively little. The amount of heat absorbed in the drop is then determined mostly by the R/δ ratio which decreases with time due to a decrease in the drop radius. Figure 1(b) shows that the decrease of the drop radius in the modeled case is not very high, less than 20% of R_o. Therefore, the decrease in the absorbed heat is also low, and, as shown in Figs. 1(c) and (d), the evaporation rate decreases relatively slowly. In the final part of the vaporization process, the drop leaves the solenoid and the amplitude of the magnetic field decreases rapidly. The heat absorbed in the drop is not sufficient to maintain its high temperature and both the temperature and the net evaporation rate begin to decrease until the melting point is reached.

Although the character of $T(t)$ curves for the three models is similar for identical external parameters of the vaporization process, the absolute values of temperatures display very significant differences. In the near-plateau region, the temperatures computed

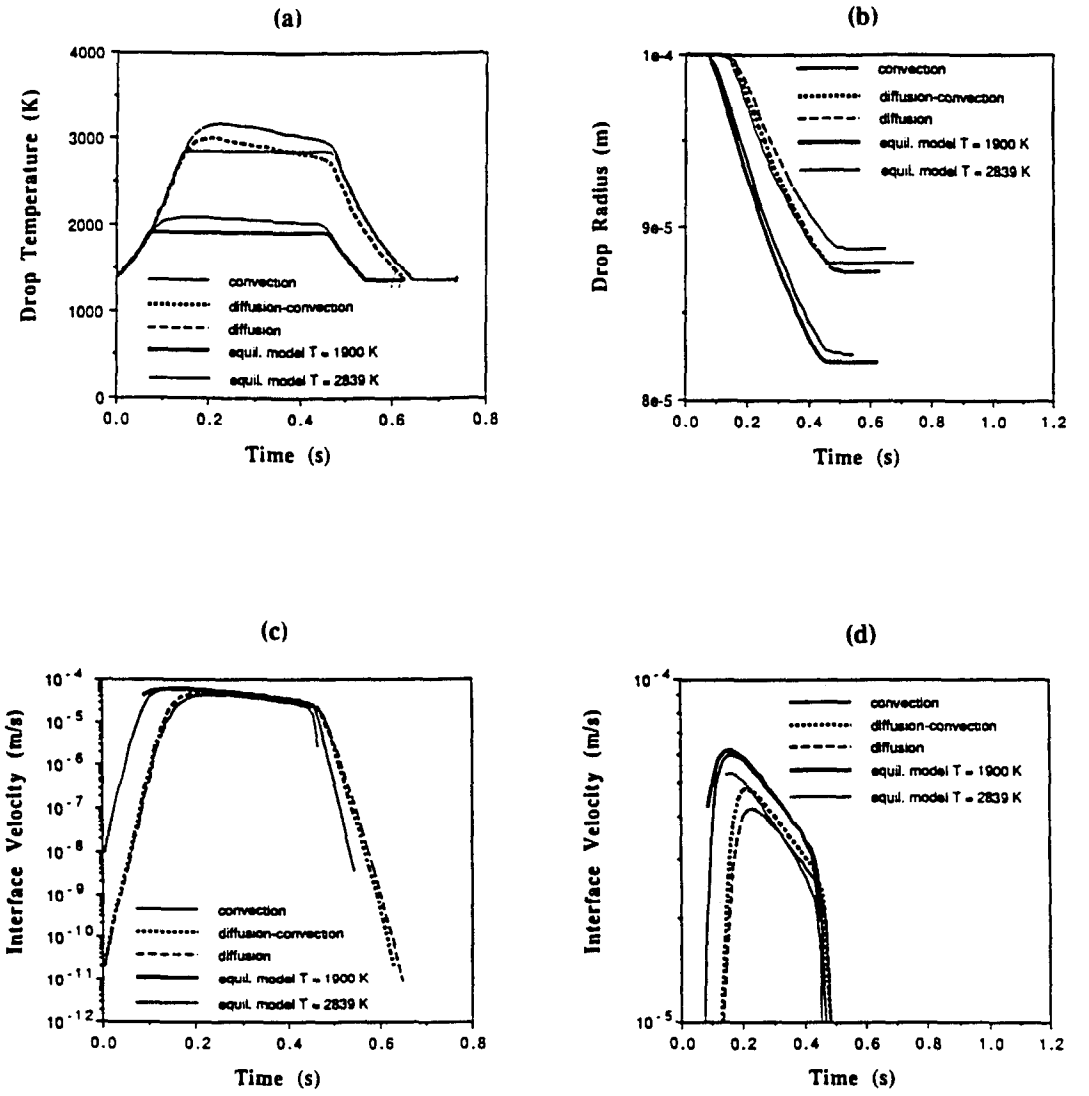

FIG. 1. Drop temperature (a), drop radius (b), interface velocity (c and d) vs time for various vaporization models, $I_0 = 500$ A, $\omega = 2\pi \times 10^7\ s^{-1}$, $R_0 = 10^{-4}$ m, $v_g = 0$.

by the DM are more than 1000 K higher than the temperatures obtained by the HVM. This is a logical consequence of the fact that with the HVM, the vapor is immediately removed from the surface and the drop can freely evaporate as if in vacuum while with the DM, the process is driven by the diffusion of the metal vapor into the surrounding gas. The DCM falls between these two limiting cases. The values of temperatures in the near-plateau region were about 150 K lower than in the diffusion limit. The difference is caused by the convective removal of the vapor from the surface due to the fall of the drop through the solenoid. The drop velocity is not very high, particularly due to the Lorentz forces acting against gravity in the upper part of the solenoid. Therefore, the $T(t)$ curve obtained by the DCM is much closer to the diffusion limit than to the high-velocity limit, as shown in Fig. 1(a). Similar behavior was observed in Fig. 1(c) for interface velocities. This is a consequence of the character of the given functional relationships $dR/dt = f(T)$ for all the three models. Note that the HVM shows an evaporation rate that is higher by 2–3 orders of magnitude than the DM when the process begins. Later the difference is only about 20–30% as shown in Fig. 1(d), which presents the highest part of the $dR(t)/dt$ curve in detail. This is caused by the different character of the $dR/dt = f(T)$ curves for the DM and the HVM.

The final size of the drop radius, which is the most important parameter from the point of view of technical applications, was only 6.9% lower for the HVM than the corresponding value for the DM, as shown in Fig. 1(b).

We also investigated the influence of the velocity v_g

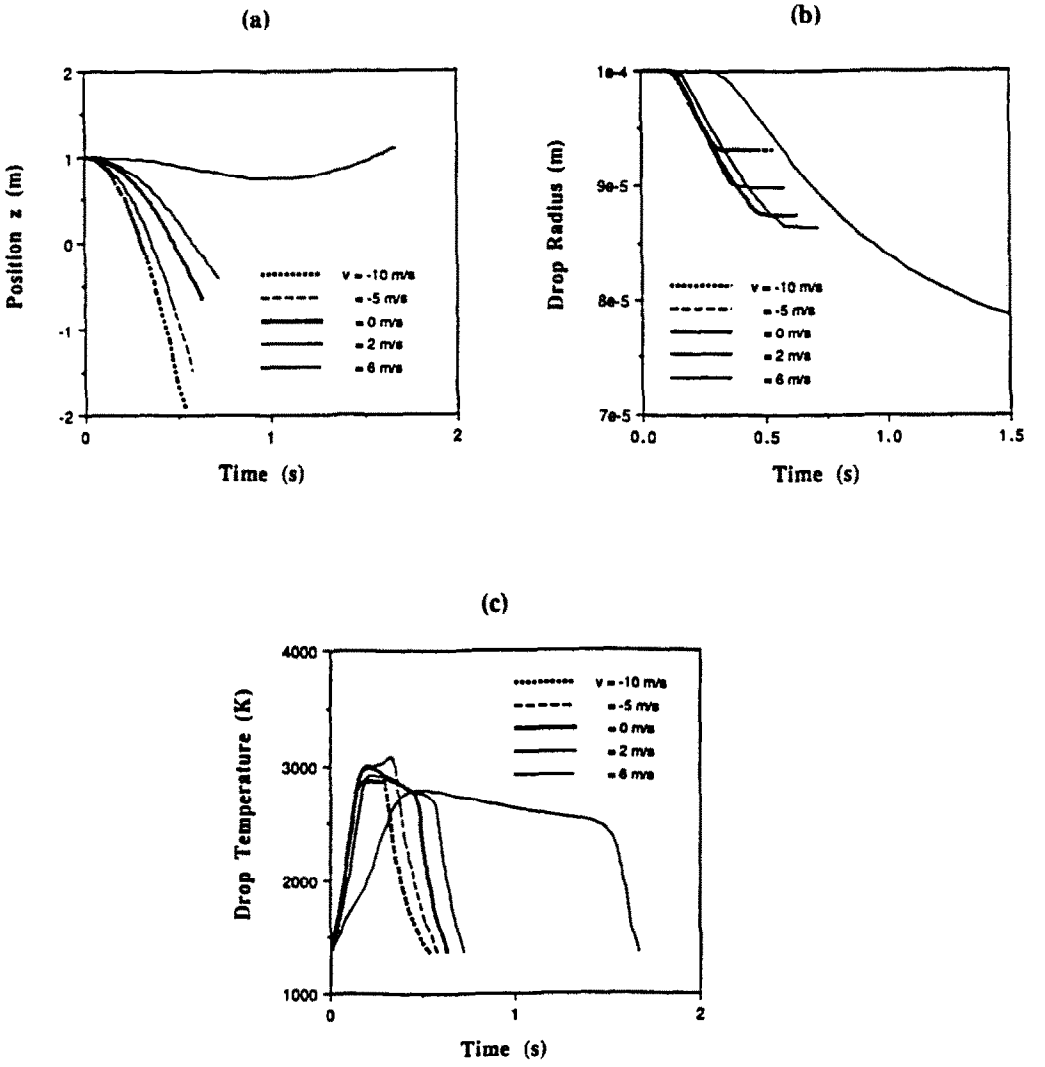

FIG. 2. Drop position (a), drop radius (b), and drop temperature (c) vs time for the diffusion–convection model, $I_0 = 500$ A, $\omega = 2\pi \times 10^7\ s^{-1}$, $R_0 = 10^{-4}$ m and various v_g.

of ambient gas on the evaporation process using the diffusion–convection model. Figure 2(a) shows that the character of drop motion in the z-direction is different for different v_g. Due to the drag forces, the ambient gas flowing through the solenoid in the direction of gravity (minus sign in Fig. 2(a)) pushes droplets down and increases their velocity in the z-direction. The droplets stay inside the solenoid for a shorter time, and consequently, the vaporization process is less effective. Figure 2(b) shows, for example, the final size of the drop radius R_f for $v_g = -10\ m\ s^{-1}$ is about 6% higher than for $v_g = 0$. In general, the flow of ambient gas against the motion of droplets has a positive influence on the vaporization process. Due to increasing time of stay of the droplet inside the solenoid, its size reduction is higher than for $v_g = 0$. For $v_g = 2\ m\ s^{-1}$, the final size drop radius is about 1.5% lower than for $v_g = 0$. However, there exists a limiting value, v_{gl}, of v_g. For $v_g > v_{gl}$, the droplets are ejected from the solenoid by the Lorentz and drag forces. In our modeled case it was $v_{gl} = 4\ m\ s^{-1}$. Apparently, for lower I_0 and ω, v_{gl} is higher because the Lorentz forces supporting the drop against gravity are smaller.

The influence of v_g on the drop temperature history is shown in Fig. 2(c). The highest temperatures are reached for small negative v_g when v_g is close to the velocity of the droplet fall, and consequently the evaporation process is near-diffusion driven. The peak on the $T(t)$ curve for $v_g = -5\ m\ s^{-1}$ means that at this time, the diffusion limit is reached because the velocity of the gas is very close to the velocity of the droplet. The lowest drop temperatures occur for $v_g = 6\ m\ s^{-1}$. The drop remains inside the device for a period two times longer than for $v_g = 2\ m\ s^{-1}$. Also, the efficiency of the vaporization process was best, as shown in Fig.

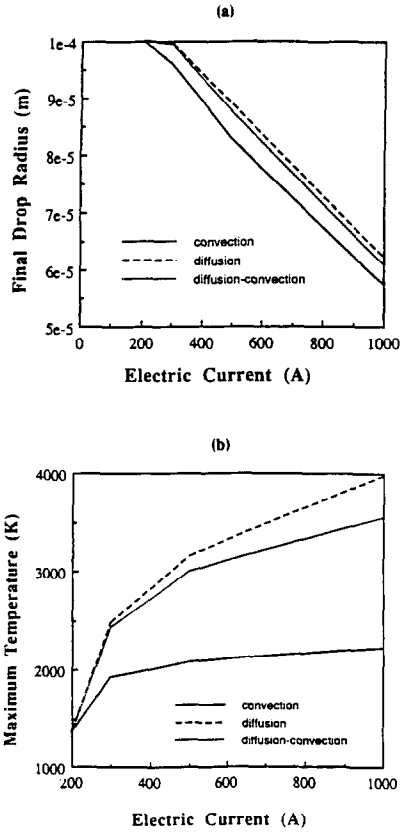

FIG. 3. Dependence of the final size of drop radius R_f (a) and the maximum temperature of the drop T_{max} (b) on the amplitude of alternating electric current in the solenoid, $\omega = 2\pi \times 10^7\ s^{-1}$, $R_0 = 10^{-4}$ m, $v_g = 0$ and various vaporization models.

2(b). However, as seen in Fig. 2(a), the droplet was finally ejected out of the solenoid because $v_g > v_{gl}$.

We also analyzed the influence of the amplitude I_0 and radian frequency ω of the applied alternating electric current in the solenoid. Figures 3(a) and (b) show the influence of I_0 on the final drop radius, R_f, and the maximum drop temperature, T_{max}, respectively, computed for various models with $v_g = 0$ and $\omega = 2\pi \times 10^7\ s^{-1}$. The threshold value of I_0 to obtain measurable changes in the drop radius is in the range between $I_0 = 200$ and 300 A for all the three models. The differences in R_f between the DM and HVM are less than 10% in the region $I_0 \in (300\ A, 1000\ A)$.

Figure 3(b) further shows that for higher values of I_0 ($I_0 > 500$ A for the given radian frequency $\omega = 2\pi \times 10^7\ s^{-1}$), the maximum temperatures of the drop can be above the boiling point when computed by the DM and DCM. Using the relations (28) or (34) to compute interface velocity, however, may not be correct above T_b. Thus, different model treatments should be used here (see, e.g. ref. [15]).

Figure 4 shows the influence of ω on R_f and T_{max} for the DCM with $I_0 = 1000$ A, $v_0 = 2\ m\ s^{-1}$. The threshold value of ω was found to be $\omega_t = 2.0 \times 10^7$

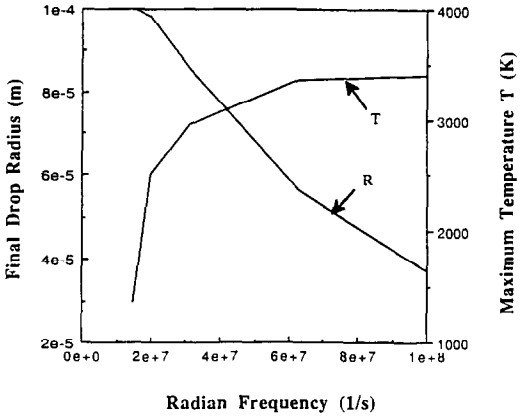

FIG. 4. Dependence of the final size of drop radius R_f and the maximum drop temperature T_{max} on the radian frequency of the applied current, computed by DCM, $I_0 = 1000$ A, $R_0 = 10^{-4}$ m, $v_g = 2\ m\ s^{-1}$.

s^{-1}. For higher ω, we also observed (as in the case of higher I_0) the drop temperatures higher than T_b, the 'safe' region with $T < T_b$ was relatively narrow, $\omega \in (2.0 \times 10^7\ s^{-1}, 3.0 \times 10^7\ s^{-1})$.

5. DISCUSSION

We compared the results obtained by the three non-equilibrium models with the computations performed by the equilibrium vaporization model (EM) from [19]. Figure 1(a) shows that the EM with $T_{vap} = 1900$ K gives temperature histories relatively similar to the HVM, also final values of the drop radius differ very little, less than 1%, as seen in Fig. 1(b). Comparison of the curves $T(t)$ and $dR(t)/dt$ for both models in Figs. 1(a) and (d) shows that in the near-plateau region of the HVM, the interface velocities computed by the EM are higher in the first half of the region. The differences are less than 3%. Later, the velocities computed by the EM are lower by up to 2%. The physical reason for these differences lies in the fact that for the HVM, the temperature of the drop increases (though very slowly) in the first part of the near-plateau region. Therefore, the absorbed heat is spent partially to heat the drop and the interface velocity is smaller than that for the EM. In the subsequent phase, the temperature of the drop computed by the HVM is decreasing and the heat released during this process can be used partially for vaporization. The velocities then are higher than for the EM.

When we chose the vaporization temperature in the EM to be equal to the boiling point, $T_{vap} = 2839$ K, we obtained the results similar to the DCM with $v_g = 0$ as seen from Figs. 1(a)–(d). The difference in R_f between the DCM and EM is only 1%, and also the histories of the drop radius differ very little. The differences in interface velocities exhibit a similar character as the differences between the HVM and EM with $T_{vap} = 1900$ K described before. The absolute

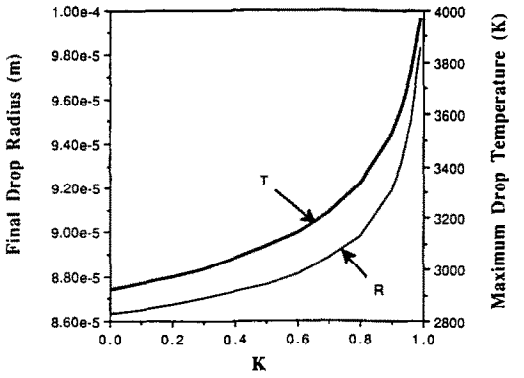

FIG. 5. Influence of the factor $K = \rho_s/\rho_\infty$ on the final size of drop radius and maximum drop temperature, $I_0 = 500$ A, $\omega = 2\pi \times 10^7\ s^{-1}$, $R_0 = 10^{-4}$ m, $v_g = 2\ m\ s^{-1}$.

values of the differences, however, are up to 10% higher.

Therefore, it follows from our analysis, that in the usual technical applications, the equilibrium vaporization model with a properly chosen vaporization temperature is sufficiently accurate in the temperature region between the melting and boiling point.

In this paper, we have dealt only with a single droplet and stagnant surroundings. In the real situation, there may be interactions between the droplets and the vapor content ρ_∞ in the surroundings may increase if we assume continuous vaporization with slower flow of ambient gas. We estimated the possible influence of the increasing ρ_∞ on our results by putting

$$\rho_\infty = K\rho_s, \tag{37}$$

where $K \in \langle 0, 1 \rangle$. Figure 5 shows the dependence of the final size of the drop radius, R_f, and the maximum drop temperature, T_{max} on K for $v_g = 2\ m\ s^{-1}$ with all other parameters being the same as in our basic set of computations. The functions $R_f = R_f(K)$ and $T_{max} = T_{max}(K)$ exhibit a similar character. For smaller K, approximately $K < 0.5$, both the functions are slowly, almost linearly increasing with increasing K, e.g. the difference between R_f for $K = 0$ and 0.5 is less than 2%. For higher K, the increase in R_f and T_{max} is faster and the vaporization process becomes much less effective.

6. CONCLUSIONS

Three nonequilibrium models were formulated to study evaporation of molten-metal drops moving through an inhomogeneous alternating magnetic field. An analysis of two limiting cases in the determination of evaporation rate, the vacuum-like high-velocity model and diffusion model, showed that the differences in drop temperatures for these limits can be very high (up to 1000 K). However, only relatively small differences (less than 10%) in the final size of the drop radius R_f, which is the most important parameter from the point of view of technical applications, were observed.

The influence of the flow velocity v_g of ambient gas in the direction opposite to the gravity was investigated by a quasi-steady diffusion–convection model and found to be generally positive. The improvement in the efficiency of the process was up to 4% accounting for R_f. However, there always exists an upper limit to v_g, v_{gl}. For $v_g > v_{gl}$, the drop is ejected from the electromagnetic-field generator. The influence of v_g acting in the direction of gravity was always negative due to a significant decrease in the duration of droplet residence time within the vaporization chamber.

Comparison of the three nonequilibrium models with the equilibrium model from ref. [19] showed that in a realistic range of parameters of external magnetic field, the results obtained by the equilibrium model were very close to the corresponding values for the vacuum-like nonequilibrium model when lower vaporization temperatures T_{vap} were chosen. Higher T_{vap} in the equilibrium model (close to the boiling point) gave results similar to the diffusion–convection model with $v_g = 0$. An equilibrium vaporization model with a properly chosen vaporization temperature is, therefore, sufficiently accurate for the usual technical applications.

Acknowledgement—This paper is based upon work supported by Texas Advanced Technology Program, under grant number 003604-027. The authors wish to acknowledge constructive discussions with U. B. Sathuvalli and V. G. Stickel.

REFERENCES

1. N. A. Fuchs, *Evaporation and Droplet Growth in Gaseous Media*. Pergamon Press, New York (1959).
2. A. Williams, Combustion of droplets of liquid fuels: a review, *Combust. Flame* **21**, 1–31 (1973).
3. J. C. Kent, Quasi-steady diffusion-controlled droplet evaporation and condensation, *Appl. Sci. Res.* **28**, 315–360 (1973).
4. G. M. Faeth, Current status of droplet and liquid combustion, *Prog. Energy Comb. Sci.* **3**, 191–224 (1977).
5. C. K. Law, Recent advances in droplet vaporization and combustion, *Prog. Energy Comb. Sci.* **8**, 169–199 (1982).
6. W. A. Sirignano, Fuel droplet vaporization and spray combustion, *Prog. Energy Comb. Sci.* **9**, 291–322 (1982).
7. S. Prakash and W. A. Sirignano, Theory of convective droplet vaporization with unsteady heat transfer in the circulating liquid phase, *Int. J. Heat Mass Transfer* **23**, 253–268 (1980).
8. S. K. Aggarawal, A. Y. Tong and W. A. Sirignano, A comparison of vaporization models in spray combustion, *AIAA J.* **22**, 1448–1457 (1984).
9. B. Abramzon and W. A. Sirignano, Approximate theory of a single droplet vaporization in a convective field: effects of variable properties, Stefan flow and transient liquid heating. In *Proceedings of the 1987 ASME–JSME Thermal Engng Joint Conf.* (Edited by P. J. Marta and I. Tanasawa), Vol. 1, pp. 11–18. JSME Tokyo and ASME New York (1987).
10. S. K. Aggarwal, G. Chen, T. A. Jackson and G. L. Switzer, Vaporization behavior of fuel droplets in a hot air stream, *Int. J. Heat Mass Transfer* **34**, 2669–2673 (1991).
11. A. Berlemont, M.-S. Grancher and G. Gonesbet, On

the Lagrangian simulation of turbulence influence on droplet evaporation, *Int. J. Heat Mass Transfer* **34,** 2805–2812 (1991).
12. I. N. Tang and H. R. Munkelwitz, Determination of vapor pressure from droplet evaporation kinetics, *J. Coll. Int. Sci.* **141,** 109–118 (1991).
13. S. Zhang and G. Gogos, Film evaporation of a spherical droplet over a hot surface: fluid mechanics and heat/mass transfer analysis, *J. Fluid Mech.* **222,** 543–563 (1991).
14. A. Block-Bolten and T. W. Eagar, Metal vaporization from weld pools, *Metall. Trans. B* **15B,** 461–469 (1984).
15. T. DebRoy, S. Basu and K. Mundra, Probing laser induced metal vaporization by gas dynamics and liquid pool transport phenomena, *J. Appl. Phys.* **70,** 1313–1319 (1991).
16. Y. Bayazitoglu and R. Cerny, Vaporization of molten-copper drops due to alternating electromagnetic field, *Proceedings of the First International Conference on Transport Phenomena in Processing* (Edited by S. I. Guceri), pp. 899–913 (1992); also in *J. Mat. Proc. Mfg Sci.* **1**(2), 227–244 (1992).
17. Y. Bayazitoglu and R. Cerny, Electromagnetic vaporization of molten-metal drops, *Int. J. Heat Mass Transfer* **36,** 277–286 (1993).
18. Y. Bayazitoglu, R. Cerny and I. Sengupta, Production of very fine metal particles in an electromagnetic vaporization device, *Proceedings of ASME Winter Annual Meeting*, HTD-vol. 233, pp. 23–33, November (1992).
19. R. Cerny and Y. Bayazitoglu, Numerical simulation of electromagnetic melting and evaporation of spherical metal particles, *Numerical Heat Transfer, Int. J. Computation Methodology* (in press).
20. W. R. Smythe, *Static and Dynamic Electricity* (3rd Edn). McGraw-Hill, New York (1968).
21. E. A. Kennard, *Kinetic Theory of Gases*. McGraw-Hill, New York (1938).
22. E. A. Brandes (ed.), *Smithells Metals Reference Book* (6th Edn). Butterworths, London (1983).
23. I. Langmuir, Evaporation of small spheres, *Phys. Rev.* **12,** 368–370 (1918).
24. T. K. Sherwood and R. L. Pigford, *Absorption and Extraction*. McGraw-Hill, New York (1952).
25. S. L. Soo, *Multiphase Fluid Dynamics*. Science Press and Gower Technical, Hong Kong (1990).
26. S. Chapman and T. G. Cooling, *The Mathematical Theory of Non-Uniform Gases* (3rd Edn). Cambridge Univ. Press, Cambridge (1970).
27. D. E. Gray (ed.), *American Institute of Physics Handbook*. McGraw-Hill, New York (1972).
28. Y. S. Touloukian and D. P. de Witt, *Thermophysical Properties of Matter*, Vol. 7. IFI/Plenum, New York (1970).
29. B. F. Armaly, T. S. Chen and N. Ramachandran, Correlations for mixed convection flows across horizontal cylinders and spheres, *ASME J. Heat Transfer* **110,** 511–514 (1989).